


ARTICLE

Open Access



Development of morpholine ring-bearing halogenated α,β -unsaturated ketones as selective monoamine oxidase-B inhibitors

Jiseong Lee^{1†}, Saranya Kattil Parmbil^{2†}, Nagendar Kumar Pandit², Sunil Kumar², Asad Syed³, Abdallah M. Elgorban³, Ling Shing Wong⁴, Ranjana⁵, Hoon Kim^{1*}  and Bijo Mathew^{2*}

Abstract

Nine morpholine-derived halogenated chalcone derivatives (**MHC1-MHC9**) were synthesized, and their inhibitory activity against monoamine oxidase (MAO) was evaluated. **MHC5** showed the highest inhibitory activity against MAO-B with an IC_{50} value of 0.065 μ M, followed by **MHC7** (IC_{50} = 0.078 μ M) and **MHC6** (IC_{50} = 0.082 μ M). The *para*-F substituent **MHC4** was also potent (IC_{50} = 0.095 μ M). The selectivity index values of all the compounds were high for MAO-B over MAO-A, and the values for **MHC5** and **MHC4** were 66.15 and 80.11, respectively. **MHC5** and **MHC4** were competitive MAO-B inhibitors with K_i values of 0.024 ± 0.00062 and 0.041 ± 0.0028 μ M, respectively. In reversibility tests, the changes in residual activity before and after the dialysis of **MHC5** and **MHC4** were similar to those of safinamide, a reversible MAO-B reference inhibitor. Additionally, molecular docking and dynamic simulations predicted that the lead molecules **MHC5** and **MHC4** could strongly bind to the MAO-B active site with docking scores of -10.92 ± 0.08 and -10.64 ± 0.14 kcal/mol, respectively. Additionally, **MHC4** and **MHC5** exhibited favorable ADME features, including blood–brain barrier permeability. The experiments confirmed that **MHC5** and **MHC4** are reversible and potent selective inhibitors of MAO-B and are promising candidates for the treatment of neurodegenerative diseases (human health).

Keywords Morpholine, Chalcone, Monoamine oxidase, Reversibility, Kinetics, Molecular dynamics, ADME analysis

[†]Jiseong Lee and Saranya Kattil Parmbil have contributed equally to this work.

*Correspondence:

Hoon Kim

hoon@sunchon.ac.kr

Bijo Mathew

bijomathew@aims.amrita.edu; bijovilaventgu@gmail.com

¹ Department of Pharmacy, and Research Institute of Life Pharmaceutical Sciences, Sunchon National University, Suncheon 57922, Republic of Korea

² Department of Pharmaceutical Chemistry, Amrita School of Pharmacy, AIMS Health Sciences Campus, Amrita Vishwa Vidyapeetham, Kochi 682 041, India

³ Department of Botany and Microbiology, College of Science, King Saud University, P.O. 2455, Riyadh 11451, Saudi Arabia

⁴ Faculty of Health and Life Sciences, INTI International University, 71800 Nilai, Malaysia

⁵ School of Pharmacy, Graphic Era Hill University, Dehradun 248002, India

Introduction

Monoamine oxidases (MAOs) substantially inactivate various biogenic amines in central and peripheral tissues [1]. Several neuropsychiatric and neurodegenerative disorders, such as Alzheimer's disease (AD) and Parkinson's disease (PD) are primary treatment targets of these enzymes [2]. MAO-A and MAO-B are two isoenzymes found on the mitochondrial outer membrane that produce hydrogen peroxide [3]. The quest for selective MAO inhibitors is currently a crucial focus in the field of drug discovery. Understanding the catalytic mechanism, substrate selectivity, and inhibitor-binding mode can accelerate the development of selective MAO inhibitors [4]. Early-stage PD was successfully and safely treated with monotherapy using MAO-B inhibitors. In contrast, adjuvant MAO-B inhibitors are routinely used to treat severe

diseases [5]. Significant progress has been made in the development of selective MAO-B inhibitors during the last five years, including outcomes, structures, structure–activity correlations (SARs), and medicinal chemistry approaches [6].

The MAO-B inhibitor selegiline, which is used either alone in monotherapy or in combination with levodopa, is effective in treating the symptoms of PD. First-pass metabolism converts selegiline into R(-)amphetamine and R(-)methamphetamine, which may have detrimental effects on the cardiovascular and neurological systems [7]. The third-generation MAO-B inhibitor safinamide, a reversible and selective MAO-B inhibitor, has favorable pharmacokinetic and pharmacodynamic features for the treatment of PD [8]. Recently, several studies have suggested that many structural scaffolds exhibit remarkable MAO-B inhibition with a reversible and competitive mode of inhibition. These include chalcones, pyrazolines, isatins, coumarins, chromones, and benzyloxy-derived compounds [9–18].

Chalcones are bioactive compounds containing carbonyl-conjugated systems and two electrophilic sites. These traditional substances are the biogenetic antecedents of various therapeutically useful substances, including flavonoids and isoflavonoids [19]. Chalcones have *cis* and *trans* isomers owing to the presence of olefinic bonds, although the thermodynamically more stable *trans* form is more prevalent. Additionally, this unusual conjugated form of ketones serves as a Michael acceptor

in several cellular biochemical signaling pathways [20]. The physicochemical properties of chalcones, which are provided by the components that make up the complete molecule, are directly related to how well they block selective MAO-B enzymes [11]. Many chalcones linked to FDA-approved drugs have recently shown remarkable MAO-B inhibition [21–24]. The electrophilic nature of the enone unit of chalcones is influenced by the differential electron density of the aromatic and heterocyclic nuclei caused by the presence of different substituents [11]. The ongoing efforts over the past several years to develop potent MAO-B inhibitors have led to the identification of novel compounds. However, based on the aforementioned data, the parent chalcone scaffold continued to play a significant role in inhibiting MAO-B.

Morpholine is a tetrahydro-1,4-oxazine containing a saturated heterocyclic ring. It is a nonplanar heterocyclic structure comprising two ethylene bridges connecting electronegative oxygen and nitrogen atoms. The morpholine ring is an integral part of central nervous system (CNS)-acting FDA-approved drugs such as phendimetrazine-anorectic, moclobemide-reversible MAO-A inhibitor, reboxetine-antidepressant, and rocuronium-neuromuscular agents (Fig. 1) [25]. Recently, morpholine-containing chalcones were shown to exhibit potent and selective MAO-B inhibitory activity [26, 27]. The current study focuses on the MAO inhibitory effect of the morpholine heterocyclic system on the *para*

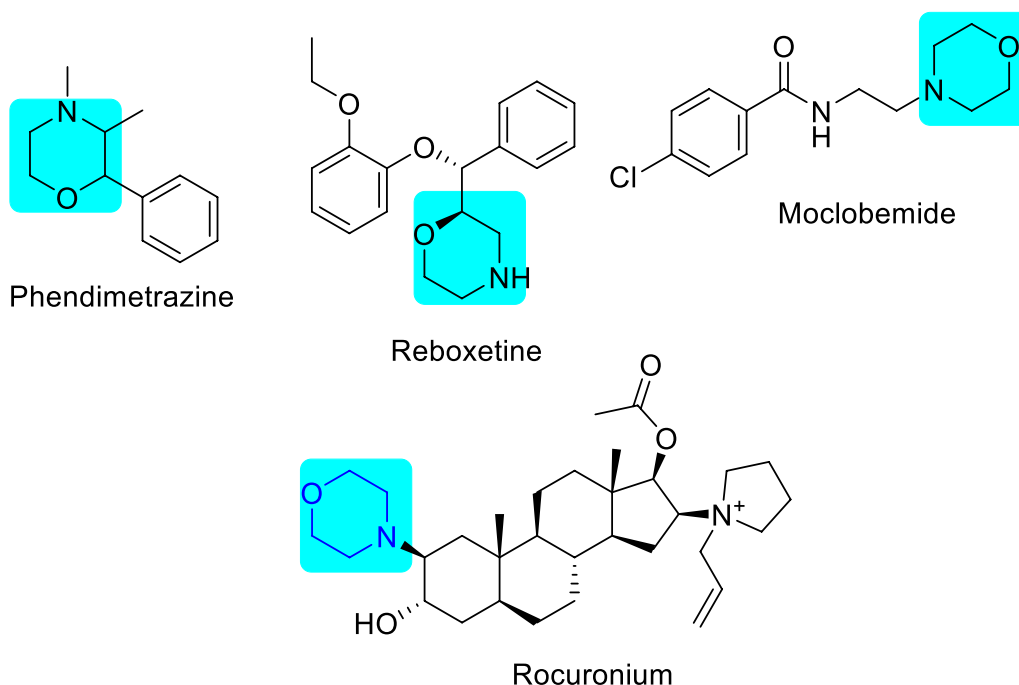
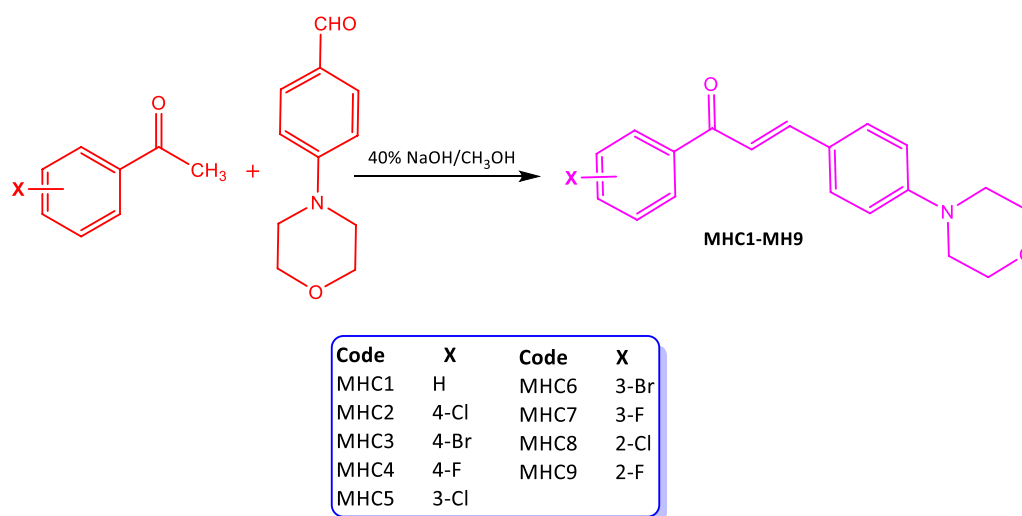


Fig. 1 Morpholine structure-based drugs approved by FDA



Scheme 1 Synthetic route of halogenated chalcones bearing morpholine ring

position of ring **B** of the phenyl system and the fine-tuning of various halogens on the phenyl ring **A** in the chalcones.

Materials and methods

Synthesis

Equimolar amounts of 4(4-formylphenyl) morpholine (0.01 M) and the corresponding acetophenones (0.01 M) were combined in a beaker and dissolved in 7.5 mL of 40% NaOH and 15–20 mL of methanol. The reaction mixture was stirred for 14–24 h using a magnetic stirrer. After completion of the reaction, ice cubes were added to the mixture and the precipitate was collected. The product was filtered and rinsed with ice-cold water to remove excess base. Methanol was used to recrystallize the product. The synthesis route is shown in Scheme 1.

(2E)-3-[4-(morpholin-4-yl)phenyl]-1-phenylprop-2-en-1-one (MHC1)

^1H NMR (500 MHz, CDCl_3): δ 8.00–7.99 (d, 2H), 7.78–7.75 (d, 1H), 7.57–7.53 (m, 3H), 7.49–7.46 (d, 2H), 7.39–7.36 (d, 1H), 6.89–6.87 (d, 2H), 3.86–3.84 (m, 4H), 3.26–3.24 (m, 4H); ^{13}C NMR (125 MHz, CDCl_3) δ 190.63, 152.77, 145.03, 144.02, 138.76, 132.41, 130.15, 128.54, 128.39, 125.82, 118.73, 114.64, 66.64, 48.00. Molecular formula $\text{C}_{19}\text{H}_{19}\text{NO}_2$ (HRMS) Calculated=293.3596, Observed=293.3595. Elemental analysis calculated: C, 77.79; H, 6.53; N, 4.77; O, 10.91, Observed: C, 77.81; H, 6.51; N, 4.74; O, 10.94.

(2E)-1-(4-chlorophenyl)-3-[4-(morpholin-4-yl)phenyl]prop-2-en-1-one (MHC2)

^1H NMR (500 MHz, CDCl_3): δ 7.95–7.93 (d, 2H), 7.78–7.75 (d, 1H), 7.57–7.54 (d, 2H), 7.46–7.43 (m, 2H), 7.34–7.31 (d, 1H), 6.89–6.87 (d, 2H), 3.86–3.84 (m,

4H), 3.27–3.25 (m, 4H); ^{13}C NMR (125 MHz, CDCl_3) δ 189.18, 152.88, 145.25, 138.74, 137.06, 130.26, 129.80, 128.82, 125.56, 118.03, 114.58, 66.63, 47.92. Molecular formula $\text{C}_{19}\text{H}_{18}\text{ClNO}_2$ (HRMS) Calculated=327.8047, Observed=327.8046. Elemental analysis calculated: C, 69.62; H, 5.53; Cl, 10.81; N, 4.27; O, 9.76, Observed: C, 69.61; H, 5.554; Cl, 10.80; N, 4.30; O, 9.74.

(2E)-1-(4-bromophenyl)-3-[4-(morpholin-4-yl)phenyl]prop-2-en-1-one (MHC3)

^1H NMR (500 MHz, CDCl_3): δ 7.88–7.85 (m, 2H), 7.78–7.75 (d, 1H), 7.63–7.60 (m, 2H), 7.57–7.54 (d, 2H), 7.33–7.30 (d, 1H), 6.90–6.87 (m, 2H), 3.86–3.84 (m, 4H), 3.28–3.26 (m, 4H); ^{13}C NMR (125 MHz, CDCl_3) δ 189.40, 152.89, 145.60, 137.49, 131.80, 130.27, 129.93, 127.40, 125.55, 118.01, 114.58, 66.63, 47.92. Molecular formula $\text{C}_{19}\text{H}_{18}\text{BrNO}_2$ (HRMS) Calculated=372.2557, Observed=372.2556. Elemental analysis calculated: C, 61.30; H, 4.87; Br, 21.46; N, 3.76; O, 8.60, Observed: C, 61.30; H, 4.87; Br, 21.46; N, 3.76; O, 8.60.

(2E)-1-(4-fluorophenyl)-3-[4-(morpholin-4-yl)phenyl]prop-2-en-1-one (MHC4)

^1H NMR (500 MHz, CDCl_3) δ : 8.05–8.02 (m, 2H), 7.78–7.75 (d, 1H), 7.57–7.55 (d, 2H), 7.36–7.33 (d, 1H), 7.17–7.13 (m, 2H), 6.90–6.87 (d, 2H), 3.86–3.84 (m, 4H), 3.27–3.25 (m, 4H); ^{13}C NMR (125 MHz, CDCl_3) δ : 199.87, 166.40, 164.39, 152.79, 145.20, 135.06, 135.04, 130.95, 130.87, 130.19, 125.69, 116.16, 115.68, 115.51, 114.63, 47.98. Molecular Formula $\text{C}_{19}\text{H}_{18}\text{FNO}_2$ (HRMS) Calculated=311.35012, Observed=311.3501. Elemental analysis calculated: C, 73.30; H, 5.83; F, 6.10; N, 4.50; O, 10.28, Observed: C, 73.31; H, 5.82; F, 6.09; N, 4.51; O, 10.29.

2E)-1-(3-chlorophenyl)-3-[4-(morpholin-4-yl)phenyl]**prop-2-en-1-one (MHC5)**

¹H NMR (500 MHz, CDCl₃) δ: 7.96–7.95 (m, 1H), 7.87–7.86 (m, 1H), 7.79–7.76 (d, 1H), 7.57–7.52 (d, 2H), 7.52–7.51 (m, 1H), 7.43–7.47 (m, 1H), 7.32–7.26 (m, 1H), 6.89–6.87 (d, 2H), 3.86–3.84 (m, 4H), 3.28–3.26 (m, 4H); ¹³C NMR (125 MHz, CDCl₃) δ: 189.10, 152.94, 145.86, 140.40, 134.70, 132.29, 130.35, 129.86, 128.86, 126.44, 125.46, 117.95, 115.75, 77.32, 77.07, 47.89. Molecular Formula C₁₉H₁₈ClNO₂ (HRMS) Calculated=327.8047, Observed=327.8046. Elemental analysis calculated: C, 69.62; H, 5.53; Cl, 10.81; N, 4.27; O, 9.76, Observed: C, 69.60; H, 5.54; Cl, 10.82; N, 4.28; O, 9.75.

(2E)-1-(3-bromophenyl)-3-(4-morpholinophenyl)**prop-2-en-1-one (MHC6)**

¹H NMR (500 MHz, CDCl₃) δ: 8.12–8.11 (d, 1H), 7.92–7.90 (d, 1H), 7.79–7.76 (d, 1H), 7.68–7.66 (m, 1H), 7.58–7.56 (m, 2H), 7.37–7.34 (d, 1H), 7.31–7.28 (d, 1H), 6.90–6.88 (d, 2H), 3.86–3.85 (m, 4H), 3.28–3.26 (m, 4H); ¹³C NMR (125 MHz, CDCl₃) δ: 189.00, 152.93, 145.89, 140.60, 135.18, 131.36, 130.34, 126.86, 125.46, 122.84, 117.91, 114.54, 66.60, 47.88. Molecular Formula C₁₉H₁₈BrNO₂ (HRMS) Calculated=372.2557, Observed=372.2557. Elemental analysis calculated: C, 61.30; H, 4.87; Br, 21.46; N, 3.76; O, 8.60, Observed: C, 61.28; H, 4.89; Br, 21.44; N, 3.77; O, 8.61.

(2E)-1-(3-fluorophenyl)-3-[4-(morpholin-4-yl)phenyl]**prop-2-en-1-one (MHC7)**

¹H NMR (500 MHz, CDCl₃) δ: 7.80–7.77 (m, 2H), 7.69–7.68 (m, 1H), 7.57–7.56 (d, 2H), 7.48–7.44 (m, 1H), 7.33–7.30 (d, 1H), 7.27–7.25 (m, 1H), 6.90–6.88 (d, 2H), 3.86–3.84 (m, 4H), 3.28–3.26 (m, 4H); ¹³C NMR (125 MHz, CDCl₃) δ: 189.16, 163.85, 161.88, 152.92, 140.91, 130.12, 125.52, 119.42, 115.27, 115.57, 77.03, 77.07, 76.79, 47.91. Molecular Formula C₁₉H₁₈FNO₂ (HRMS) Calculated=311.3501, Observed=311.3500. Elemental analysis calculated: C, 73.30; H, 5.83; F, 6.10; N, 4.50; O, 10.28, Observed: C, 73.28; H, 5.84; F, 6.11; N, 4.52; O, 10.26.

(2E)-1-(2-chlorophenyl)-3-[4-(morpholin-4-yl)phenyl]**prop-2-en-1-one (MHC8)**

¹H NMR (500 MHz, CDCl₃) δ: 7.49–7.48 (m, 2H), 7.45–7.43 (m, 2H), 7.40–7.35 (m, 3H), 6.97–6.94 (d, 2H), 6.87–6.84 (m, 2H), 3.85–3.83 (m, 4H), 3.27–3.25 (m, 4H); ¹³C NMR (125 MHz, CDCl₃) δ: 193.99, 152.98, 146.80, 139.61, 131.20, 130.99, 130.34, 130.20, 129.23, 126.70, 125.19, 123.10, 114.53, 77.30, 77.05, 76.79, 47.86. Molecular Formula C₁₉H₁₈ClNO₂ (HRMS) Calculated=327.8080, Observed=327.8046. Elemental

analysis calculated: C, 69.62; H, 5.53; Cl, 10.81; N, 4.27; O, 9.76, Observed: C, 69.60; H, 5.52; Cl, 10.80; N, 4.28; O, 9.77.

(2E)-1-(2-fluorophenyl)-3-[4-(morpholin-4-yl)phenyl]**prop-2-en-1-one (MHC9)**

¹H NMR (500 MHz, CDCl₃) δ: 7.80–7.76 (m, 1H), 7.70–7.66 (m, 1H), 7.55–7.52 (m, 2H), 7.51–7.46 (m, 1H), 7.26–7.21 (m, 2H), 7.16–7.12 (m, 1H), 6.89–6.86 (m, 2H), 3.86–3.84 (m, 4H), 3.27–3.25 (m, 4H); ¹³C NMR (125 MHz, CDCl₃) δ: 189.18, 162.01, 160.00, 152.87, 145.24, 133.43, 130.88, 127.74, 125.56, 124.42, 122.43, 116.53, 116.34, 114.57, 66.63, 47.93. Molecular formula C₁₉H₁₈FNO₂ (HRMS) Calculated=311.3501, Observed=311.3501. Elemental analysis calculated: C, 73.30; H, 5.83; F, 6.10; N, 4.50; O, 10.28, Observed: C, 73.32; H, 5.84; F, 6.09; N, 4.48; O, 10.27.

Biochemistry**Inhibition studies of MAO-A and MAO-B**

The activities of MAO-A and MAO-B were assayed using kynuramine (0.06 mM) and benzylamine (0.30 mM), respectively, by continuously measuring the changes in absorbance at 316 and 250 nm, respectively [28]. Toloxatone, clorgyline, safinamide, and pargyline were used as reference compounds. Recombinant human MAO-A, MAO-B, benzylamine, kynuramine, safinamide mesylate salt, pargyline, clorgyline, and tolaxatone were purchased from Sigma-Aldrich (St. Louis, MO, USA).

Enzyme kinetics

The enzyme activity of MAO-B was assayed at five substrate concentrations around the K_m value (0.0375 – 0.6 μM) without inhibitor for enzyme kinetics. Inhibition kinetics were determined prior to the inhibition study. As an initial screening step, residual activity was analyzed by measuring the change in absorbance in the presence of the inhibitor at 10 μM. IC₅₀ values were determined for potential compounds with residual activity of less than 80% from residual activity curves that were plotted using GraphPad Prism software 5 (San Diego, CA, USA) [29]. The limit of IC₅₀ was set to 40 μM. If necessary, a concentration of 1 μM was used for potent inhibitors. The selectivity index (SI) of MAO-B was calculated by dividing IC₅₀ of MAO-A / IC₅₀ of MAO-B [30]. The type of inhibition of the leading compound for MAO-B was determined at three inhibitor concentrations, ~1/2×, 1×, and 2×IC₅₀, as well as at five different substrate concentrations [31]. Enzyme kinetic patterns and K_i values were determined by comparing Lineweaver–Burk (LB) plots and their secondary plots [32].

Reversibility studies

The reversibilities of the leading compounds for MAO-A and MAO-B were evaluated by comparing the undialyzed (A_U) and dialyzed (A_D) residual activities at a concentration approximately twice the IC_{50} after preincubation for 30 min before measurement. The time-dependency curve was constructed by measuring the residual activity after preincubation for 0, 5, 10, 20, 30, and 60 min at the concentration, and the preincubation time was selected. Two types of reference inhibitors were used for MAO-A and MAO-B: reversible inhibitors toloxatone and safinamide mesylate (for MAO-A and MAO-B, respectively) and irreversible inhibitors clorgyline and pargyline (for MAO-A and MAO-B, respectively) [33]. A dialysis kit (6–8 kDa, DiaEasy™) was purchased from BioVision (St. Louis, MA, USA).

Computational studies

Molecular docking

A molecular docking study of the lead compounds, **MHC5** and **MHC4** from the enzyme inhibition analysis was conducted using the Schrödinger suite [34]. The X-ray structure of human MAO-B (hMAO-B, PDB ID:2V5Z) was obtained from the Protein Data Bank [35]. The protein preparation wizard from the Schrödinger suite, which also performed energy minimization, hydrogen atom addition, protonation state correction, and protonation state addition, was used to enhance and optimize the crystal structures. The ligand structure was constructed using the LigPrep software. The automated center of the grid box comprised the co-crystallized ligands. The Extra Precision (XP) docking protocol default parameters and Force Field OPLS4 default settings were applied to the docking simulations [36, 37].

Molecular dynamic simulation

The molecular dynamics (MD) simulations were conducted using Schrodinger LLC's Desmond simulation program (Shaw, 2021). For the Desmond system builder panel, a protein–ligand combination was initially developed utilizing the compounds **MHC5** and **MHC4** against MAO-B using an aqueous solvent system. The simulation parameters were 100 ns at 300 K, 1.01325 bar pressure, and 1000 frames for full protein–ligand simulations and stability trajectory analysis such as root-mean-square deviation (RMSD), root mean square fluctuation (RMSF), and protein–ligand interactions [36, 37].

MM-GBSA

The Molecular Mechanics Generalized Born and Surface Area (MM-GBSA) solvation method was employed to calculate the binding energies of ligands to proteins. Multiple poses from molecular dynamics (MD) simulations

of the docked complex were utilized to assess both macromolecular stability and the affinity between proteins and ligands. The free energy was determined using the specified formula during the post-processing stage following the MD studies.

$$G = E_{\text{int}} + E_{\text{ele}} + E_{\text{vdw}} + G_{\text{pol}} + G_{\text{np}} - TS$$

The molecular mechanics framework designates the internal, electrostatic, and van der Waals energies as E_{int} , E_{ele} , and E_{vdw} , respectively. The equation includes representations for the free energy contributions of polar and non-polar solvation systems, indicated by G_{pol} and G_{np} , respectively. S stands for an entropy estimate, and T represents the absolute temperature. The formula employed to calculate the binding free energy, ΔG_{Bind} , between the ligand and the protein is as follows:

$$\Delta G_{\text{Bind}} = (G_{\text{PL}}) - (G_{\text{p}}) - (G_{\text{L}})$$

where PL is the complex, p is the protein, and L is the ligand.

ADME prediction

The ADME of a potential therapeutic agent is considered throughout the drug discovery process to ensure appropriate pharmacokinetic parameters. Using web-based software such as SwissADME (<http://www.swissadme.ch/>) and pkCSM (<http://biosig.unimelb.edu.au/pkcsm/>), pharmacokinetic parameters were determined in silico [38, 39].

Results and discussion

Chemistry

To synthesize morpholine-containing unsaturated ketones, benzaldehyde-based morpholines, and appropriate halogen-derived methyl ketones were combined using the Claisen-Schmidt condensation method in the presence of an alcoholic basic medium (Scheme 1). The H_1 and H_2 protons of the morpholine ring resonated at 3.28–3.23 and 3.83–3.86 ppm as triplets, respectively, according to the ^1H NMR spectra of **MHC1**–**MHC9**. Chalcones containing morpholine had sharp doublets of H_α and H_β protons at 7.33–7.58 and 7.80–7.70 ppm, respectively. The large coupling constant of 15 Hz indicated a double bond in the *trans* configuration of the chalcones. The existence of a sharp deshielded sp^2 carbonyl carbon at 193–189 ppm and the morpholine ring containing $(\text{CH}_2)\text{-N}$, and $(\text{CH}_2)\text{-O}$ carbon of shielded area range between 40 and 70 ppm in the ^{13}C -NMR data supported the hypothesis that the compound was an α , β -unsaturated ketone system. Owing to the nature of the targeted compounds, all chalcones containing

morpholine exhibited intense molecular ions in their mass spectra (Additional file 1).

Enzyme inhibition studies

Inhibition studies of MAO-A and MAO-B

All compounds tested showed low residual activity of <50% for MAO-B at a concentration of 1 μM , while six showed low residual activity of <50% for MAO-A at 10 μM (Table 1). **MHC5** had an IC_{50} value of 0.065 μM , showing the greatest inhibitory ability against MAO-B, followed by compounds **MHC7** (IC_{50} =0.078 μM) and **MHC6** (IC_{50} =0.082 μM). The compound with the highest MAO-A inhibitory activity was **MHC2**, with an IC_{50} of 0.82 μM . All the compounds showed higher inhibitory activity against MAO-B compared to MAO-A, with high SI values for MAO-B. The SI value of **MHC8** was 102.47, followed by **MHC4** (80.11) and **MHC5** (66.15). Comparing the **MHC** series of compounds with reference compounds for MAO-B inhibition, **MHC5** had lower potency than safinamide (a reversible MAO-B inhibitor); however, it had similar or better potency than pargyline (an irreversible MAO-B inhibitor).

All the compounds in the present study were chalcone-based derivatives with a morpholine ring bonded to the **B**-ring. Previously, we synthesized 1-(4-morpholinophenyl) prop-2-en-1-one (chalcones). In this design strategy, a morpholine ring was placed on the **A** ring of chalcones, and various electron-donating and electron-withdrawing groups were added to the *para* position of the phenyl **B** ring of the basic scaffold.

The **MHC** series contained different substituents based on the type and location of the halogen atom in

the **A**-ring of chalcone. Considering the IC_{50} values, we found that the MAO-B inhibitory effect was the best when a halogen was bonded to the *meta*-site of ring **A**, compared to the *para*- or *ortho*-sites, which had similar IC_{50} values. When comparing the *meta*-derivative sites, the inhibitory ability was in the order of $-\text{Cl} > -\text{F} > -\text{Br}$, although the difference was insignificant. The structure–activity relationships (SARs) are shown in Fig. 2.

Enzyme kinetics

Enzyme kinetics and inhibition studies were performed at five substrate concentrations and three inhibitor concentrations for *para*-Cl substituted **MHC5** and *meta*-F substituted **MHC4**. In the Lineweaver-Bulk plot, **MHC5** and **MHC4** appeared to be competitive MAO-B inhibitors (Fig. 3A, C). From the secondary plots, the K_i values of both compounds were found to be 0.024 ± 0.00062 and 0.041 ± 0.0028 μM , respectively (Fig. 3B, D). These results suggested that **MHC5** and **MHC4** are acting as competitive inhibitors of MAO-B.

Reversibility studies

The reversibility of MAO-B inhibition by **MHC5** and **MHC4** was analyzed using the dialysis method after 30 min of pre-incubation. The preincubation time was selected as 30 min, based on their time-dependency studies (Additional file 1: Figure S10). Concentrations of **MHC5**, **MHC4**, safinamide, and pargyline used were twice their IC_{50} values (0.13, 0.19, 0.038, and 0.22 μM , respectively). Recovery patterns were compared using undialyzed (A_U) and dialyzed (A_D) relative activities. The inhibition of MAO-B by compounds **MHC5** and **MHC4** recovered

Table 1 Inhibitions of MAO-A and MAO-B by chalcone derivatives

Compound	Residual activity (%)		IC_{50} (μM)		SI
	MAO-A (10 μM)	MAO-B (1 μM)	MAO-A	MAO-B	
MHC1	51.15 \pm 0.87	4.35 \pm 1.44	11.97 \pm 0.27	0.21 \pm 0.010	57.00
MHC2	26.14 \pm 2.55	19.74 \pm 7.44	0.82 \pm 0.25	0.13 \pm 0.01	6.31
MHC3	50.56 \pm 2.21	23.42 \pm 6.41	11.67 \pm 1.38	0.17 \pm 0.04	68.65
MHC4	28.16 \pm 4.06	-7.98 \pm 3.76	7.61 \pm 0.19	0.095 \pm 0.012	80.11
MHC5	23.55 \pm 2.42	0.02 \pm 1.55	4.30 \pm 0.043	0.065 \pm 0.014	66.15
MHC6	15.47 \pm 5.50	7.10 \pm 0.61	3.04 \pm 0.068	0.082 \pm 0.012	37.07
MHC7	24.63 \pm 3.59	-3.11 \pm 1.89	2.89 \pm 0.62	0.078 \pm 0.007	37.05
MHC8	72.93 \pm 1.68	7.20 \pm 2.33	15.37 \pm 0.81	0.15 \pm 0.02	102.47
MHC9	20.28 \pm 2.06	-1.60 \pm 2.26	4.28 \pm 0.052	0.13 \pm 0.05	32.92
Toloxatone	-	-	1.65 \pm 0.094	>40	0.041
Safinamide	-	-	>40	0.019 \pm 0.0019	2105.26
Clorgyline	-	-	0.008 \pm 0.001	2.43 \pm 0.71	0.0033
Pargyline	-	-	2.15 \pm 0.23	0.11 \pm 0.01	19.55

Data were analyzed with independent duplicate or triplicate experiments and presented as the means \pm standard error. The selectivity index (SI) was expressed for MAO-B using IC_{50} values, that is, IC_{50} of MAO-A/ IC_{50} of MAO-B

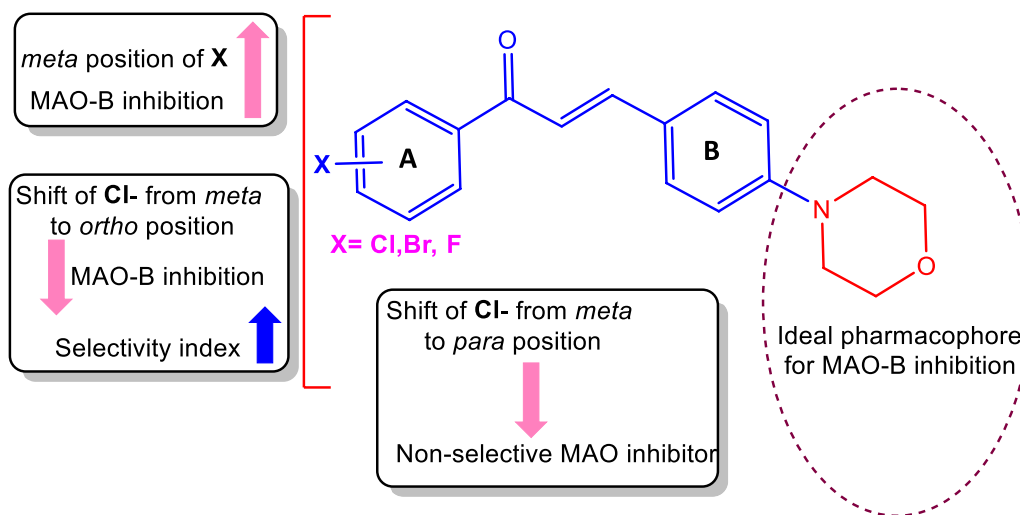


Fig. 2 SARs of morpholine-based compounds

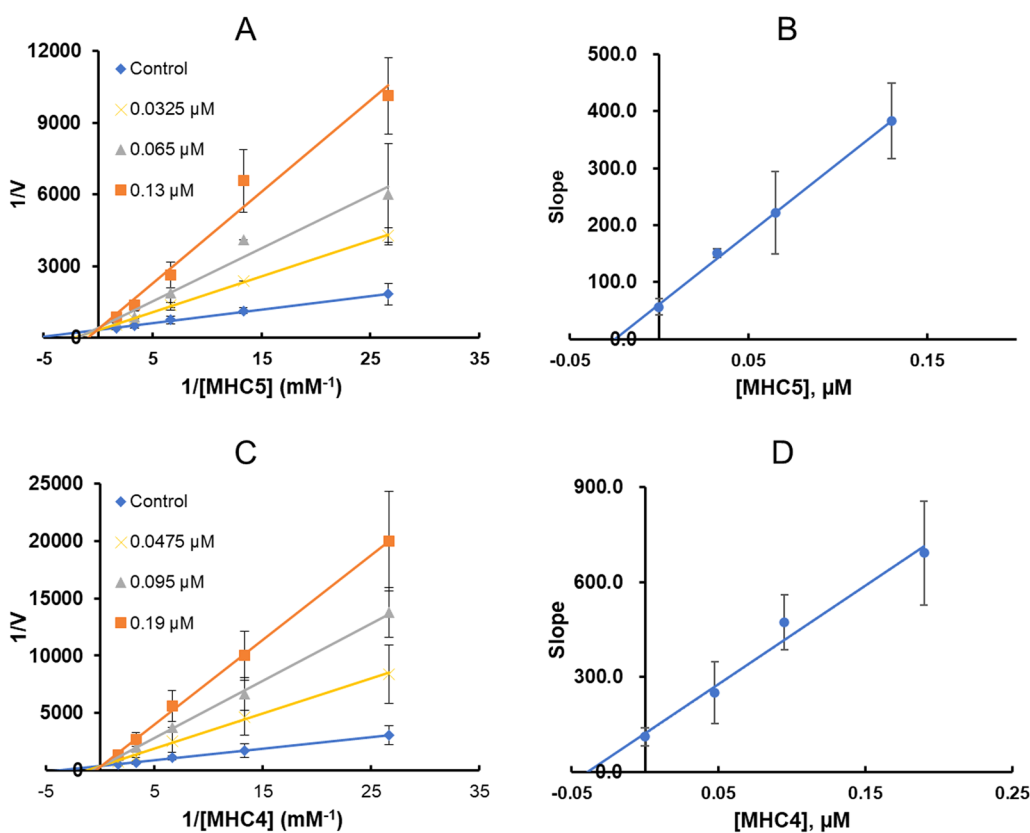


Fig. 3 Lineweaver–Burk plots for MAO-B inhibitions by MHC5 (A) and MHC4 (C), and their respective secondary plots (B and D) of the slopes vs. inhibitor concentrations

from 17.35% to 72.39% and from 9.02% to 74.70%, respectively (Fig. 4). The recovery of the compound was similar to that of safinamide (reversible type, 24.98–70.03%) and

could be distinguished from that of pargyline (irreversible type, 20.76–10.35%). These results suggested that MHC5 and MHC4 are reversible inhibitors of MAO-B.

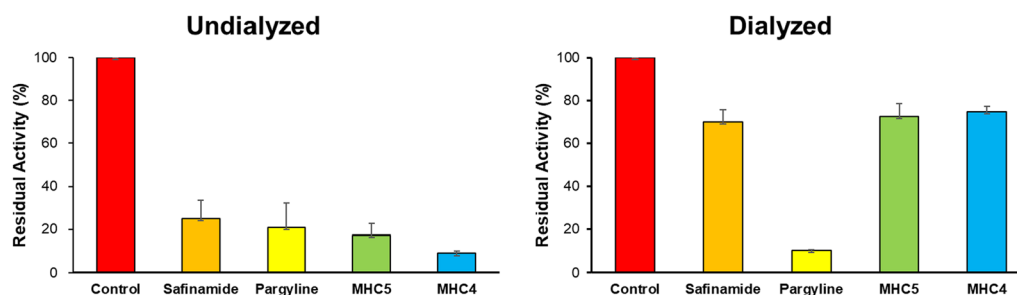


Fig. 4 Recovery of MAO-B inhibition by **MHC5** and **MHC4** in residual activities measured using dialysis experiments

Table 2 Docking scores of the lead molecules along with a reference molecule

Compound	Docking score (kcal/mol)
MHC4	-10.643 ± 0.14
MHC5	-10.915 ± 0.08
MHC6	-10.078 ± 0.10
MHC7	-10.498 ± 0.12
Safinamide	-11.313 ± 0.13

Values were obtained using the XP mode

Computational studies

Molecular docking

Using molecular docking, we further analyzed the hypothetical binding modes of the lead compounds (**MHC4**, **MHC5**, **MHC6**, and **MHC7**) as effective selective MAO-B inhibitors. Using the Glide module, we docked successful compounds from virtual screening into the binding cavity of 2V5Z. Using increased precision (XP), we examined the hits which showed docking scores ranging from -10.915 to -10.078 kcal/mol (Table 2). To validate the docking approach, we co-crystallized the ligand in the binding site of 2V5Z with 0.90 Å RMSD. The binding affinities of these substances were comparable to that of the co-crystallized ligand (safinamide, XP = -11.313 kcal/mol). As shown in Fig. 6, all lead molecules were bound to the same binding site of the co-crystallized ligand.

In the binding site of 2V5Z, **MHC5** and **MHC4** interacted with important amino acids, such as Tyr60, Phe99, Pro102, Phe103, Phe104, Trp119, Leu164, Leu167, Phe168, Leu171, Cys172, Tyr188, Ile198, Ile199, Gln206, Tyr398, Tyr435, Ile316, Tyr326, Leu328, and Phe343 (Fig. 5). In particular, Tyr326 interacted through pi-pi stacking with the phenyl ring attached to morpholine in both ligands (**MHC5** and **MHC4**). Analysis of the orientation of all lead molecules revealed that their A rings were in close proximity to the FAD cofactor (Fig. 6).

MD simulation

MD simulation is a widely used and well-known method that aids in our understanding of the stability and interaction of enzyme-ligand complexes in the process of computer-aided drug development. We used 100 ns MD simulations on the best lead molecules, **MHC5** and **MHC4** to determine the stability of the receptor-ligand complex interacting inside the 2V5Z binding pocket after performing molecular docking against MAO-B.

Root mean square deviation (RMSD) The root-mean-square deviation (RMSD) value derived from the MD simulation trajectory is one of the most crucial markers for identifying multiple structural conformations of the protein backbone over time during system equilibration. A stable protein structure is represented by low and stable RMSD values. The protein should be close to equilibrium, which means that the RMSD value should remain constant to evaluate the ligand-protein interaction. A comparison of the RMSD of lead and the reference molecule with that of MAO-B is shown in Fig. 7. RMSD was used to measure the alpha carbon atoms in the protein backbone and evaluate the stability of the protein throughout the simulation. The average RMSD values for **MHC5** and **MHC4** were 2.79 and 2.37, respectively. Both lead compounds exhibited similar behavior throughout the 100 ns. At 20–35 ns after stabilization, the **MHC5** cells showed a visual change. In the case of **MHC4**, modest variations were observed between 10 and 30 ns and between 40 and 60 ns. Therefore, it can be concluded that **MHC5** differs slightly from **MHC4** in its interactions; however, overall, both molecules exhibited stability in protein-ligand complexes.

Root mean square fluctuation (RMSF) The flexibility and mobility of particular amino acids are described by the root mean square fluctuation (RMSF). Given the reduced RMSF, the residue might have been less active and mobile. It may be argued that the bond between the protein and ligand is stronger when the RMSF value is low at residues near the active site or at residues where the ligand inter-

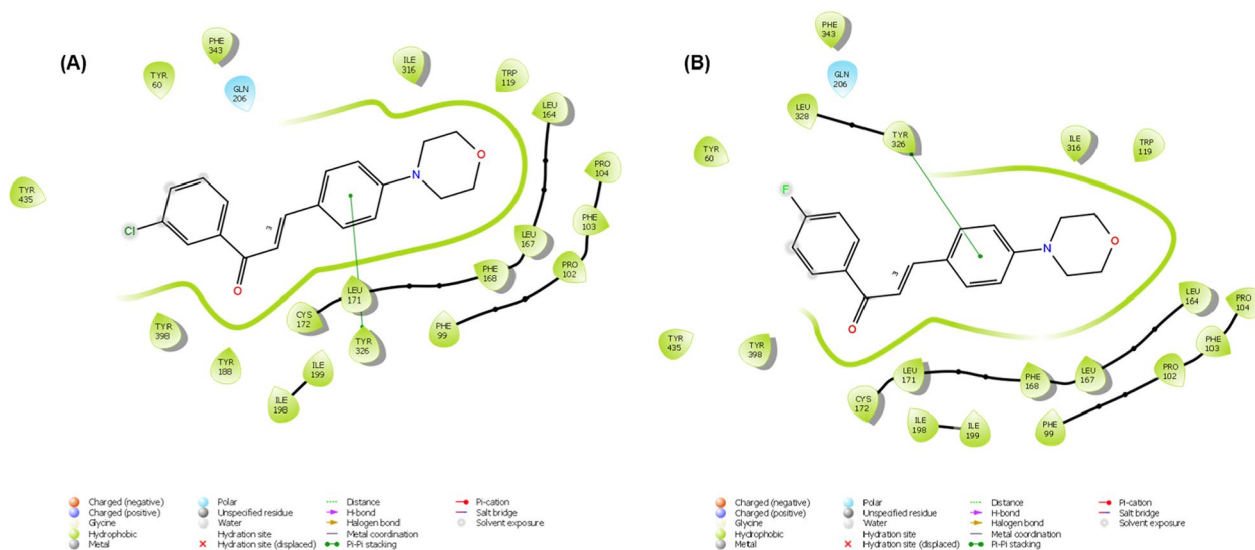


Fig. 5 2D interaction of MHC5 (A) and MHC4 (B) with MAO-B binding pocket

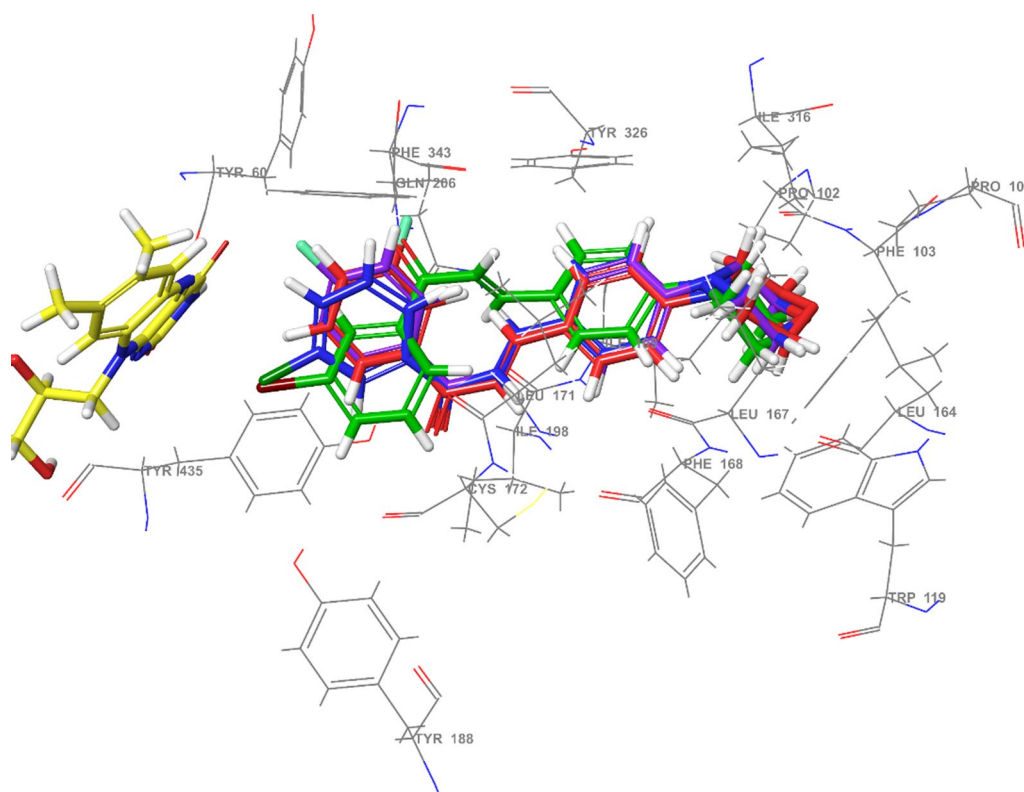


Fig. 6 3-D Superimposition of all ligands that bind close to the FAD cofactor (yellow). MHC4, MHC5, MHC6, and MHC7 are represented by the colors, violet, blue, green, and red, respectively

acts with the receptor protein. Higher values (peaks) indicate the existence of twists, loose bonding loops, terminal ends, and loose bonding, demonstrating the flexibility of

the structure. Low values indicated secondary structures such as β -sheets and α -helices, which suggested structural stability. The RMSF variation for MHC5 and MHC4 with

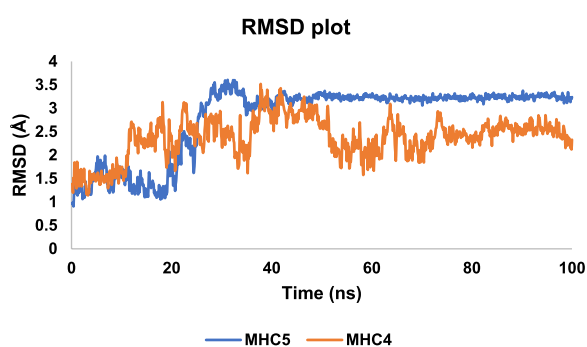


Fig. 7 RMSD plots of **MHC5** and **MHC4** to MAO-B

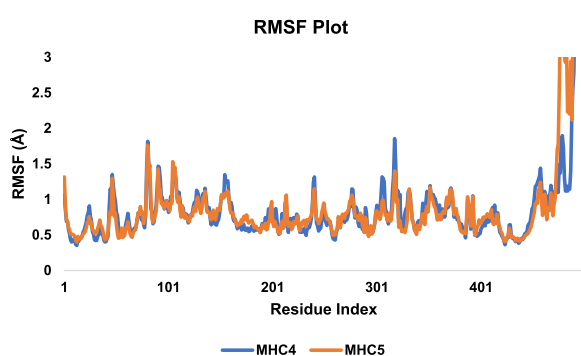


Fig. 8 RMSF plots of **MHC5** and **MHC4** to MAO-B

the 2V5Z protein was revealed to be 0.50–3.0 Å (Fig. 8). By comparing the RMSF values of both lead compounds, **MHC5** exhibited higher fluctuation than **MHC4**, i.e., overall **MHC5** and **MHC4** for 0.97 Å and 0.92 Å, respectively. When **MHC5** was simulated, important contacts were observed in 24 amino acids such as Leu88 (0.67 Å), His90 (0.76 Å), Gly101 (0.98 Å), Phe99 (0.87 Å), Pro102 (0.91 Å), Pro104 (0.83 Å), Trp119 (0.79 Å), Leu164 (0.81 Å), Leu167 (0.70 Å), Phe168 (0.66 Å), Ile171 (0.66 Å), Cys172 (0.65 Å), Tyr188 (0.58 Å), Cys192 (0.57 Å), Ile198 (0.58 Å), Ile199 (0.68 Å), Gly205 (0.69 Å), Gln206 (0.64 Å), Ile316 (0.69 Å), and Tyr326 (0.60 Å), Phe343 (0.59 Å), Leu345 (0.66 Å), Tyr398 (0.50 Å), and Tyr435 (0.45 Å). In case of **MHC4**, important contacts were in 21 amino acid such as Tyr60 (0.54 Å), His90 (0.81 Å), Pro102 (0.90 Å), Pro104 (0.85 Å), Trp119 (0.73 Å), Leu164 (0.89 Å), Leu167 (0.72 Å), Phe168 (0.66 Å), Ile171 (0.66 Å), Cys172 (0.66 Å), Ile198 (0.71 Å), Ile199 (0.86 Å), Gln206 (0.87 Å), Ile316 (0.70 Å), Tyr326 (0.66 Å), Leu328 (0.58 Å), Met341 (0.54 Å), Phe343 (0.70 Å), Leu345 (0.65 Å), Tyr398 (0.50 Å), and Tyr435 (0.44 Å). Both lead molecules with almost identical amino acids demonstrated interactions during the simulation with very minor RMSF variations.

Protein–ligand contact Hydrogen bonds are considered a crucial type of binding interaction in drug design that aids in understanding the metabolism, adsorption, and specificity of drug candidates. The pattern by which docked protein–ligand poses changed was clearly demonstrated throughout the MD simulation period, owing to the important contributions of non-covalent interactions such as hydrophobic contacts, π -cation; π - π ; polar or ionic interactions, and the creation of a water-bridge hydrogen bond. In the presence of active-site amino acid residues in the binding pocket of the 2V5Z protein, the lead molecules, **MHC5** and **MHC4** showed similar binding patterns (Fig. 9). MD simulations showed that the major interactions between chemicals and proteins were hydrophobic contacts, hydrogen bonds, and polar (water-mediated) hydrogen bonding interactions. Tyr435 and Tyr398 were crucial amino acids for the binding site, together with Phe343, Tyr326, and Leu171. These interlocking residues were discernible in the matched docked complexes, indicating that the docked ligands remained in the active pocket throughout the simulation. The catalytic pocket of 2V5Z was significantly occupied by bioactive chemicals based on protein–ligand contact mapping. Based on the number of molecular interactions generated throughout the 100 ns MD simulation time, **MHC5** and **MHC4** were determined to be potent MAO-B inhibitors. This enables the identification of the bioactive features of these molecules.

MM-GBSA

The estimation of free binding energy for the optimal molecule **MHC5**, possessing the highest docking energy and activity value prediction, was conducted based on its MD simulation frames. The total average energies for ΔG Bind, ΔG Bind H-bond, ΔG Bind Lipo, and ΔG Bind vdW were found to be -143.08 , -11.90 , -32.41 , and -116.13 , respectively, over the 10 to 100 ns MD snapshot. The analysis of these energies revealed that ΔG Bind vdW and ΔG Bind Lipo had the most significant impact on the average binding energy across all interactions, as outlined in Table 3.

Specifically, the ΔG Bind vdW values for the interactions of **MHC5** with protein complexes indicated stable van der Waals interactions with amino acid residues. Consequently, the MM-GBSA calculations, derived from MD simulation trajectories, exhibited consistency with the binding energies obtained from the docking results. Notably, the molecule demonstrated very low free binding energy, suggesting a strong binding affinity toward the receptor. As a result, it can be inferred that the **MHC5** compound exhibits robust affinity for the MAO-B protein.

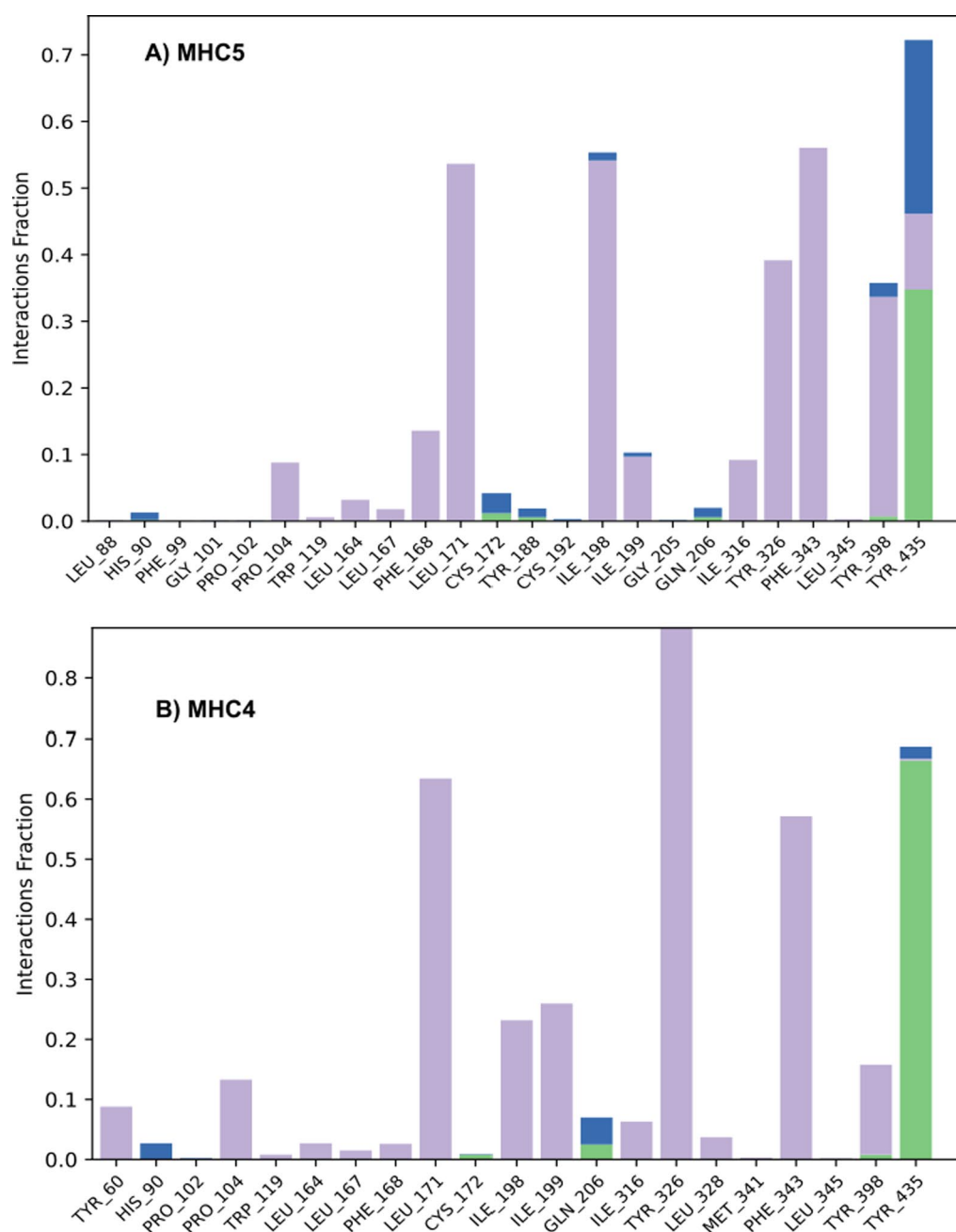


Fig. 9 Protein – ligand contact histogram analysis for **MHC5 (A)** and **MHC4 (B)**. Green, hydrogen bond; blue, water bridge; grey, hydrophobic interaction

ADME/T properties

A biologically effective molecule needs to be present at the target site in the body in a bioactive form for a sufficiently long period for the anticipated biological activities to occur for it to be effective as a medication. To produce new drugs, it is necessary to evaluate absorption, distribution, metabolism, and excretion (ADME) at progressively earlier stages of the discovery process

when the number of potential compounds is high, but physical sample access is constrained. In this context, the solubility of the preferred compounds varies from -3.58 to -4.87 , according to the logarithm of the molar concentration. Log S values of the lead compounds **MHC5** and **MHC4** were -4.56 and -4.12 log mol/L, respectively. The intake of oral medicines can be predicted based on Caco-2 cell permeation. The molecule should

Table 3 Free binding energies of the molecule **MHC5** through MM-GBSA*

MD (ns)	ΔG Bind	ΔG Bind H-bond	ΔG Bind Lipo	ΔG Bind vdW
10	-144.36	-12.34	-34.41	-114.38
20	-141.14	-10.81	-33.17	-118.75
30	-140.12	-11.76	-30.46	-113.14
40	-131.74	-11.08	-31.33	-117.30
50	-140.57	-12.18	-31.51	-114.57
60	-147.24	-12.48	-32.39	-112.18
70	-142.78	-11.59	-31.85	-116.87
80	-144.36	-12.14	-34.00	-113.66
90	-154.49	-12.58	-32.87	-117.25
100	-144.06	-12.04	-32.12	-123.21

* kcal/mol

have a P_{app} value greater than 8×10^{-6} cm/s for remarkable permeation. Interestingly, all the compounds exhibited significant permeability. If log VD_s is greater than 0.45, the medicine may be distributed particularly in tissues as compared to plasma; therefore, most of the molecules are distributed throughout the tissues. The drug is minimally attached to blood proteins according to the fraction-bound method of assessing drug efficiency and is therefore more freely distributed. The GI permeability was evaluated, and the preferred compounds exhibited high GI permeability. BBB permeation is crucial for treating neurodegenerative diseases. In this study, SwissADME and pkCSM were used to evaluate the BBB permeability (Table 4). While substances with log BB values

of -1 are assumed to be poorly distributed in the brain, substances with log BB values of >0.3 are thought to easily cross the BBB. In this study, all compounds had a value greater than 0.3. The log BB values of the lead compounds **MHC5** and **MHC4** were 0.364 and 0.422, respectively, indicating that they could easily permeate the BBB. While substances with log PS value < -3 are assumed to poorly penetrate the CNS, substances with log PS values of > -2 are thought to easily cross the CNS. All compounds investigated showed CNS permeability. Every substance uniquely interacts with cytochromes, regardless of whether it serves as a substrate or an inhibitor. The total clearances of the lead compounds **MHC5** and **MHC4** were 0.243 and 0.175 log ml/min/kg, respectively. Specifically, **MHC5** was predicted to have no hepatotoxicity. Most compounds exhibited favorable ADME characteristics, making them promising candidates (Fig. 10).

Collectively, nine halogenated chalcones bearing a morpholine ring were synthesized, and their inhibitory effects on MAOs were assessed. **MHC5** and **MHC4** are selective MAO-B inhibitors with reversible and competitive modes of inhibition. The ring B of **MHC5** and **MHC4** connected to the amino acid Tyr326 of MAO-B through a pi-pi stacking with docking scores of -10.64 and -10.95 kcal/mol, respectively, in molecular docking analysis. This could be the primary cause of the efficient inhibition of MAO-B by compounds **MHC5** and **MHC4**. These findings suggested that **MHC5** and **MHC4** have the potential to be used in the management of neurological disorders.

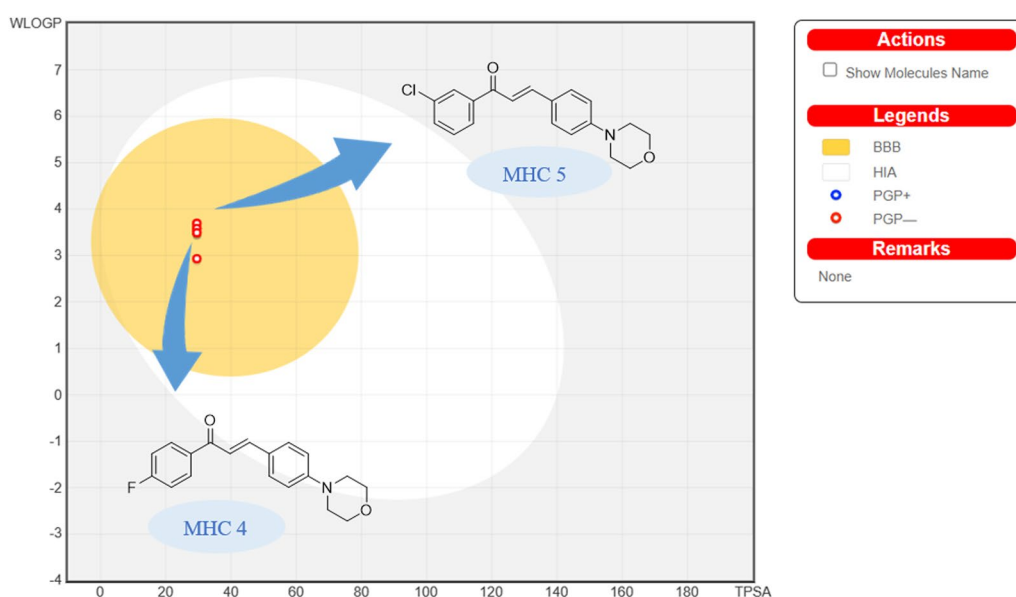
**Fig. 10** Distribution prediction of the lead compounds **MHC5** and **MHC4**

Table 4 ADME/T prediction of the MHC series

Code	Absorption			Distribution			Metabolism			Excretion total clearance (log ml/min/kg)	Hepatotoxicity	
	Log S (log mol/L)	Caco-2 perm. (logP _{app} in 10 ⁻⁶ cm/s)	Int. abs. (% absorbed)	VDss (log L/kg)	Fract. Unb (Fu)	BBB perm. (log BB)	CNS perm. (log PS)	Metabolism				
MHC1	-3.58	1.738	98.42	0.532	0	0.449	-1.399	CYP2C9, CYP3A4 Substrate CYP1A2, CYP2C19, CYP2D6 inhibitor			0.305	No
MHC2	-4.56	1.664	96.687	0.454	0	0.378	-1.411	CYP2C9, CYP3A4, CYP1A2, CYP2C19, CYP2D6 inhibitor			0.124	Yes
MHC3	-4.87	1.664	96.62	0.47	0	0.364	-1.411	CYP2C9, CYP3A4, CYP1A2, CYP2C19, CYP2D6 inhibitor			0.103	Yes
MHC4	-4.12	1.792	97.589	0.284	0	0.422	-1.438	CYP2C9, CYP3A4 Substrate CYP1A2, CYP2C19, CYP2D6 inhibitor			0.175	Yes
MHC5	-4.56	1.67	96.508	0.427	0	0.364	-1.411	CYP2C9, CYP3A4, CYP1A2, CYP2C19, CYP2D6 inhibitor			0.243	No
MHC6	-4.87	1.669	96.441	0.442	0	0.351	-1.411	CYP2C9, CYP3A4, CYP1A2, CYP2C19, CYP2D6 inhibitor			0.221	Yes
MHC7	-4.12	1.798	97.41	0.257	0	0.408	-1.438	CYP3A4 Substrate CYP1A2, CYP2C9, CYP2C19, CYP2D6 inhibitor			0.182	Yes
MHC8	-4.56	1.691	97.537	0.463	0	0.362	-1.417	CYP2C9, CYP3A4, CYP1A2, CYP2C19, CYP2D6 inhibitor			0.315	No
MHC9	-4.12	1.819	98.439	0.292	0	0.407	-1.443	CYP2C9, CYP3A4 Substrate CYP1A2, CYP2C19, CYP2D6 inhibitor			0.131	Yes

SwissADME and pkCSM were used to calculate pharmacokinetic properties in silico (<http://biosig.unimelb.edu.au/pkcsim/>). While molecules with log BB < -1 are poorly disseminated to the brain, those with log BB > 0.3 are thought to cross the BBB with ease. Compounds with log PS > -2 are thought to penetrate the CNS, whereas those with log PS < -3 are thought to be unable to do so. Perm., permeability

Supplementary Information

The online version contains supplementary material available at <https://doi.org/10.1186/s13765-024-00857-y>.

Additional file 1: Figure S1. Structure of compound **MHC 1**. Figure S1.1 | ¹H-NMR spectrum of compound **MHC 1**. Figure S1.2 | ¹³C-NMR spectrum of compound **MHC 1**. Figure S1.3 | HRMS of compound **MHC 1**. **Figure S2.** Structure of compound **MHC 2**. Figure S2.1 | ¹H-NMR spectrum of compound **MHC 2**. Figure S2.2 | ¹³C-NMR spectrum of compound **MHC 2**. Figure S2.3 | HRMS of compound **MHC 2**. **Figure S3.** Structure of compound **MHC 3**. Figure S3.1 | ¹H-NMR spectrum of compound **MHC 3**. Figure S3.2 | ¹³C-NMR spectrum of compound **MHC 3**. Figure S3.3 | HRMS of compound **MHC 3**. **Figure S4.** Structure of compound **MHC 4**. Figure S4.1 | ¹H-NMR spectrum of compound **MHC 4**. Figure S4.2 | ¹³C-NMR spectrum of compound **MHC 4**. Figure S4.3 | HRMS of compound **MHC 4**. **Figure S5.** Structure of compound **MHC 5**. Figure S5.1 | ¹H-NMR spectrum of compound **MHC 5**. Figure S5.2 | ¹³C-NMR spectrum of compound **MHC 5**. Figure S5.3 | HRMS of compound **MHC 5**. **Figure S6.** Structure of compound **MHC 6**. Figure S6.1 | ¹H-NMR spectrum of compound **MHC 6**. Figure S6.2 | ¹³C-NMR spectrum of compound **MHC 6**. Figure S6.3 | HRMS of compound **MHC 6**. **Figure S7.** Structure of compound **MHC 7**. Figure S7.1 | ¹H-NMR spectrum of compound **MHC 7**. Figure S7.2 | ¹³C-NMR spectrum of compound **MHC 7**. Figure S7.3 | HRMS of compound **MHC 7**. **Figure S8.** Structure of compound **MHC 8**. Figure S8.1 | ¹H-NMR spectrum of compound **MHC 8**. Figure S8.2 | ¹³C-NMR spectrum of compound **MHC 8**. Figure S8.3 | HRMS of compound **MHC 8**. **Figure S9.** Structure of compound **MHC 9**. Figure S9.1 | ¹H-NMR spectrum of compound **MHC 9**. Figure S9.2 | ¹³C-NMR spectrum of compound **MHC 9**. Figure S9.3 | HRMS of compound **MHC 9**. **Figure S10.** Time-dependency curves of **MHC4** and **MHC5**. The residual activities were measured at the designated times.

Acknowledgements

The authors extend their appreciation to the Researchers Supporting Project number (RSP2024R56), King Saud University, Riyadh, Saudi Arabia.

Author contributions

Conceptualization, BM and HK; synthesis, SKP, NKP, and SK; biological tests, JL; docking simulation and ADMET study, SK, AS, AME, LSW, and R.; writing—original draft preparation, JL, SK, and BM; writing—review and editing, BM and HK; supervision, BM and HK; funding acquisition, HK All authors have read and agreed to the published version of the manuscript.

Funding

This study was supported by the National Research Foundation of Korea (NRF) Grant funded by the Korean Government (NRF-2022R1A2B5B01002536), Researchers Supporting Project (RSP2024R56), King Saud University, Riyadh, Saudi Arabia.

Availability of data and materials

All data generated or analyzed during this study are included in this published article.

Declarations

Competing interests

The authors declare that they have no competing interests.

Received: 28 October 2023 Accepted: 4 January 2024

Published online: 22 January 2024

References

- Guglielmi P, Carradori S, Ammazalorso A, Secci D (2019) Novel approaches to the discovery of selective human monoamine oxidase-B inhibitors: is there room for improvement? *Expert Opin Drug Discov* 14:995–1035
- Manzoor S, Hoda N (2020) A comprehensive review of monoamine oxidase inhibitors as anti-Alzheimer's disease agents: a review. *Eur J Med Chem* 206:112787
- Ramsay RR (2013) Inhibitor design for monoamine oxidases. *Curr Pharm Des* 19:2529–2539
- Bhawna Kumar A, Bhatia M, Kapoor A, Kumar P, Kumar S (2022) Monoamine oxidase inhibitors: a concise review with special emphasis on structure activity relationship studies. *Eur J Med Chem* 242:114655
- Tan YY, Jenner P, Chen SD (2022) Monoamine oxidase-B inhibitors for the treatment of Parkinson's disease: past, present, and future. *J Parkinson's Dis* 12:477–493
- Guglielmi P, Carradori S, D'Agostino I, Campestre C, Petzer JP (2022) An updated patent review on monoamine oxidase (MAO) inhibitors. *Expert Opin Ther Pat* 32:849–883
- Finberg JP, Rabey JM (2016) Inhibitors of MAO-A and MAO-B in psychiatry and neurology. *Front Pharmacol* 7:340
- Sanchez-Alonso P, De La Casa-Fages B, Alonso-Cánovas A, Martínez-Castrillo JC (2023) Switching from rasagiline to safinamide as an add-on therapy regimen in patients with levodopa: a literature review. *Brain Sci* 13:276
- Mateev E, Georgieva M, Mateeva A, Zlatkov A, Ahmad S, Raza K, Azevedo V, Barh D (2023) Structure-based design of novel MAO-B inhibitors: a review. *Molecules* 28:4814
- Pérez-González A, Castañeda-Arriaga R, Guzmán-López EG, Hernández-Ayala LF, Galano A (2022) Chalcone derivatives with a high potential as multifunctional antioxidant neuroprotectors. *ACS Omega* 7:38254–38268
- Guglielmi P, Mathew B, Secci D, Carradori S (2020) Chalcones: unearthing their therapeutic possibility as monoamine oxidase B inhibitors. *Eur J Med Chem* 205:112650
- Mathew B, Suresh J, Anbazhagan S, Mathew GE (2013) Pyrazoline: a promising scaffold for the inhibition of monoamine oxidase. *Cent Nerv Syst Agents Med Chem* 13:195–206
- Mathew B, Parambi DGT, Sivasankarapillai VS, Uddin MS, Suresh J, Mathew GE, Joy M, Marathakam A, Gupta SV (2019) Perspective design of chalcones for the management of CNS disorders: a mini-review. *CNS Neurol Disord Drug Targets* 18:432–445
- Rangarajan TM, Mathew B (2021) Recent updates on pyrazoline derivatives as promising candidates for neuropsychiatric and neurodegenerative disorders. *Curr Top Med Chem* 21:2695–2714
- Kumar S, Nair AS, Abdelgawad MA, Mathew B (2022) Exploration of the detailed structure-activity relationships of isatin and their isomers as monoamine oxidase inhibitors. *ACS Omega* 7:16244–16259
- Koyiparambath VP, Prayaga Rajappan K, Rangarajan TM, Al-Sehemi AG, Pannipara M, Bhaskar V, Nair AS, Sudevan ST, Kumar S, Mathew B (2021) Deciphering the detailed structure-activity relationship of coumarins as Monoamine oxidase enzyme inhibitors—an updated review. *Chem Biol Drug Des* 98:655–673
- Mathew B, Mathew GE, Petzer JP, Petzer A (2017) Structural exploration of synthetic chromones as selective MAO-B inhibitors: a mini review. *Comb Chem High Throughput Screen* 20:522–532
- Sudevan ST, Rangarajan TM, Al-Sehemi AG, Nair AS, Koyiparambath VP, Mathew B (2022) Revealing the role of the benzyloxy pharmacophore in the design of a new class of monoamine oxidase-B inhibitors. *Arch Pharm (Weinheim)* 355:e2200084
- Zhuang C, Zhang W, Sheng C, Zhang W, Xing C, Miao Z (2017) Chalcone: a privileged structure in medicinal chemistry. *Chem Rev* 117:7762–7810
- Kar Mahapatra D, Asati V, Bharti SK (2019) An updated patent review of therapeutic applications of chalcone derivatives (2014-present). *Expert Opin Ther Pat* 29:385–406
- Cao Z, Yang J, Xu R, Song Q, Zhang X, Liu H, Qiang X, Li Y, Tan Z, Deng Y (2018) Design, synthesis and evaluation of 4'-OH-flurbiprofen-chalcone hybrids as potential multifunctional agents for Alzheimer's disease treatment. *Bioorg Med Chem* 26:1102–1115
- Tian C, Qiang X, Song Q, Cao Z, Ye C, He Y, Deng Y, Zhang L (2020) Flurbiprofen-chalcone hybrid Mannich base derivatives as balanced multifunctional agents against Alzheimer's disease: design, synthesis and biological evaluation. *Bioorg Chem* 94:103477
- Xiao G, Li Y, Qiang X, Xu R, Zheng Y, Cao Z, Luo L, Yang X, Sang Z, Su F, Deng Y (2017) Design, synthesis and biological evaluation of 4'-aminochalcone-rivastigmine hybrids as multifunctional agents for the treatment of Alzheimer's disease. *Bioorg Med Chem* 25:1030–1041

24. Wang L, Wang Y, Tian Y, Shang J, Sun X, Chen H, Wang H, Tan W (2017) Design, synthesis, biological evaluation, and molecular modeling studies of chalcone-rivastigmine hybrids as cholinesterase inhibitors. *Bioorg Med Chem* 25:360–371
25. Kourounakis AP, Xanthopoulos D, Tzara A (2020) Morpholine as a privileged structure: a review on the medicinal chemistry and pharmacological activity of morpholine containing bioactive molecules. *Med Res Rev* 40:709–752
26. Mathew B, Baek SC, Thomas Parambi DG, Lee JP, Mathew GE, Jayanthi S, Vinod D, Rapheal C, Devikrishna V, Kondarath SS, Uddin MS, Kim H (2019) Potent and highly selective dual-targeting monoamine oxidase-B inhibitors: fluorinated chalcones of morpholine versus imidazole. *Arch Pharm (Weinheim)* 352:e1800309
27. Sasidharan R, Eom BH, Heo JH, Park JE, Abdelgawad MA, Musa A, Gambacorta N, Nicolotti O, Manju SL, Mathew B, Kim H (2021) Morpholine-based chalcones as dual-acting monoamine oxidase-B and acetylcholinesterase inhibitors: synthesis and biochemical investigations. *J Enzyme Inhib Med Chem* 36:188–197
28. Lee HW, Ryu HW, Kang MG, Park D, Lee H, Shin HM, Oh SR, Kim H (2017) Potent inhibition of monoamine oxidase A by decursin from *Angelica gigas* Nakai and by wogonin from *Scutellaria baicalensis* Georgi. *Int J Biol Macromol* 97:598–605
29. Oh JM, Kang Y, Hwang JH, Park JH, Shin WH, Mun SK, Lee JU, Yee ST, Kim H (2022) Synthesis of 4-substituted benzyl-2-triazole-linked-tryptamine-paeonol derivatives and evaluation of their selective inhibitions against butyrylcholinesterase and monoamine oxidase-B. *Int J Biol Macromol* 217:910–921
30. Baek SC, Park MH, Ryu HW, Lee JP, Kang MG, Park D, Park CM, Oh SR, Kim H (2019) Rhamnocitrin isolated from *Prunus padus* var. *seoulensis*: a potent and selective reversible inhibitor of human monoamine oxidase A. *Bioorg Chem*. 83:317–325
31. Baek SC, Lee HW, Ryu HW, Kang MG, Park D, Kim SH, Cho ML, Oh SR, Kim H (2018) Selective inhibition of monoamine oxidase A by hispidol. *Bioorg Med Chem Lett* 28:584–588
32. Oh JM, Jang HJ, Kim WJ, Kang MG, Baek SC, Lee JP, Park D, Oh SR, Kim H (2020) Calycosin and 8-O-methylretusin isolated from *Maackia amurensis* as potent and selective reversible inhibitors of human monoamine oxidase-B. *Int J Biol Macromol* 151:441–448
33. Lee HW, Ryu HW, Kang MG, Park D, Oh SR, Kim H (2016) Potent selective monoamine oxidase B inhibition by maackiain, a pterocarpan from the roots of *Sophora flavescens*. *Bioorg Med Chem Lett* 26:4714–4719
34. Shaw DE (2021) Desmond molecular dynamics system. Maestro Desmond interoperability tools. Research, Schrodinger release. Springer, New York
35. Binda C, Wang J, Pisani L, Caccia C, Carotti A, Salvati P, Edmondson DE, Mattevi A (2007) Structures of human monoamine oxidase B complexes with selective noncovalent inhibitors: safinamide and coumarin analogs. *J Med Chem* 50:5848–5852
36. Mathew B, Haridas A, Uçar G, Baysal I, Joy M, Mathew GE, Lakshmanan B, Jayaprakash V (2016) Synthesis, biochemistry, and computational studies of brominated thienyl chalcones: a new class of reversible MAO-B inhibitors. *ChemMedChem* 11:1161–1171
37. Parambi DGT, Oh JM, Baek SC, Lee JP, Tondo AR, Nicolotti O, Kim H, Mathew B (2019) Design, synthesis and biological evaluation of oxygenated chalcones as potent and selective MAO-B inhibitors. *Bioorg Chem* 93:103335
38. Daina A, Michielin O, Zoete V (2017) SwissADME: a free web tool to evaluate pharmacokinetics, drug-likeness and medicinal chemistry friendliness of small molecules. *Sci Rep* 7:42717
39. Pires DE, Blundell TL, Ascher DB (2015) pkCSM: predicting small-molecule pharmacokinetic and toxicity properties using graph-based signatures. *J Med Chem* 58:4066–4072

Publisher's Note

Springer Nature remains neutral with regard to jurisdictional claims in published maps and institutional affiliations.